

Crystal chemistry of hydrous forsterite and its vibrational properties up to 41 GPa

ANWAR HUSHUR,¹ MURLI H. MANGHNANI,^{1,*} JOSEPH R. SMYTH,² FABRIZIO NESTOLA,³ AND DANIEL J. FROST⁴

¹Hawaii Institute of Geophysics and Planetology, University of Hawaii, Honolulu, Hawaii 96822, U.S.A.

²Department of Geological Sciences, University of Colorado, Boulder, Colorado 80309, U.S.A.

³Department of Geosciences, University of Padova, Via Giotto 1, I-35137 Padova, Italy

⁴Bayerisches Geoinstitut, Universität Bayreuth, D-95440 Bayreuth, Germany

ABSTRACT

The crystal structure of hydrous pure magnesium forsterite (Mg_2SiO_4) containing 8900 ppmw H_2O , synthesized at 12 GPa and 1250 °C, has been refined. The major hydration mechanism appears to be M1 cation vacancy with protonation of the O1–O2 octahedral edge of M1. Raman spectra up to 41 GPa show strong coupling between the two A_g modes (824.4 and 856.2 cm^{-1}). Mode Grüneisen parameters γ_i related to $\text{Mg}(2)\text{O}_6$ translation mode decrease relative to anhydrous forsterite. This is attributed to the fact that the M2 site shows full occupancy compared to the M1 site, and the vacancy predominantly occurs at the M1 site. Pressure dependencies of four OH vibrations in the region 3548–3615 cm^{-1} suggest that positional ordering of hydrogen ion (proton) takes place with increasing pressure. The OH mode at 3615 cm^{-1} shows complex response as a function of pressure: the $(\partial\nu/\partial P)$ slope changes from -0.43 below 10 GPa to 1.97 between 10 and 20 GPa, and does not show clear pressure dependence above 20 GPa. Single-crystal X-ray data were used to assign the OH band to the structural sites, O1 and O2. The proton is closer to O2 than O1. The distance between the proton and O2 is 0.96 Å. In view of the empirical relation between OH-stretching frequencies and O···O distances (Libowitzky 1999), the pressure dependence of the OH mode (3615 cm^{-1}) is well correlated with the O1–O2 distance and the degree of hydrogen bonding.

Keywords: Forsterite, X-ray diffraction, Raman spectroscopy, hydration mechanism, high pressure

INTRODUCTION

The nominally anhydrous mineral phases—olivine (α -), wadsleyite (β -), and ringwoodite [γ -(Mg,Fe) $_2\text{SiO}_4$]—in the Earth's upper mantle and transition zone (410–660 km depth) may serve as a large internal reservoir of water that has profound implications for Earth's evolution as a water planet. This concept has generated deep interest in systematic investigations of the various elastic (seismic) properties, as well as the stability of these phases as a function of water content (i.e., H content, or hydration state), crystal structure, oxidation state of Fe, and P - T environments. One of the major findings is that the effect of hydration is to decrease bulk modulus (K_0) and increase K'_0 by increasing the vacancy or unoccupied volume in the structure (e.g., Inoue et al. 1998; Jacobsen and Smyth 2006; Smyth and Jacobsen 2006). This paper represents one such step in a continued systematic investigation of the structure, vibrational properties, and compression behavior of hydrous mantle minerals.

The incorporation of hydrogen in anhydrous mineral phases occurs by bonding to lattice oxygen to form hydroxyl groups (OH^-) known in the literature as water. Much effort has been put into estimating the OH^- storage capacity of nominally anhydrous mineral phases, and to determining the factors controlling OH^- substitution and its incorporation mechanism in the lattice (Miller et al. 1987; Mackwell and Kohlstedt 1990; Rossman and Smyth

1990; Skogby et al. 1990; Bai and Kohlstedt 1993; Smyth 1994; Smyth et al. 1997; Kohlstedt et al. 1996; Matveev et al. 2001; Khisina et al. 2001; Bell et al. 2003; Braithwaite et al. 2003; Matsyuk and Langer 2004; Zhao et al. 2004; Koch-Müller et al. 2006; Mosenfelder et al. 2006; Walker et al. 2007; Bali et al. 2008). These studies have revealed that hydroxyl occurrence in mantle phases is closely related to the crystal defect structure, and that it is controlled by the diffusion rates of cations, anions, and point defects.

Although point defects have been linked to hydrogen incorporation, there remain several questions as to which point defect predominates under various conditions. Smyth (2006) has reviewed the crystal structures of the nominally hydrous and anhydrous phases that are likely constituents of Earth's mantle. In nominally hydrous silicate structures, H normally bonds to a non-silicate oxygen, that is, an oxygen not bonded to Si. There are a few examples of a proton bonded to a silicate oxygen such as in the pyroxenoids, pectolite, and serandite, but these are unusual cases in which there is an anomalously short O–O distance between unshared O atoms. In nominally anhydrous silicates, four protons may replace Si as in the hydro-garnet substitution, but this substitution has a large volume effect and is therefore destabilized by pressure (Withers et al. 1998). In pyroxenes, protonation of an oxygen atom bonded to a tetrahedral site can occur if there is some Al substitution (Smyth et al. 2007), but, again, Al substitution in tetrahedral sites is destabilized by pressure. More commonly, protonation is balanced by an octahedral

* E-mail: murli@soest.hawaii.edu

cation vacancy. In such cases, the proton is commonly located between pairs of O atoms on the side of the vacant octahedron as in olivine (Smyth 2006; Smyth et al. 2006). This substitution seems to be stabilized by pressure as the solubility of H in olivine and ringwoodite increases with pressure (Kohlstedt et al. 1996; Smyth et al. 2006; Mosenfelder et al. 2006). In the event that there is a non-silicate oxygen in a structure, it will be the first to be protonated as in wadsleyite (Smyth 1987; Jacobsen et al. 2005).

In general, vacant polyhedra are larger than occupied polyhedra so that hydrous phases are less dense than anhydrous phases. The volume effect is larger for tetrahedra than for octahedra. Furthermore, the vacant polyhedra are more compressible than those that are occupied. The proton is located on the side of the vacant polyhedron. The proton-oxygen distance is typically 0.95 to 1.05 Å, so it is always closer to one oxygen than another (Libowitzky 1999).

Olivine, (Mg,Fe)₂SiO₄, with a composition of about Fo₉₀ is considered to be the most abundant phase in the upper mantle. The olivine structure is orthorhombic (space group *Pbnm*). All O atoms are bonded to three Mg and one Si atom, and site potentials range from 26.3 V for O3 to 27.7 V for O1. Smyth et al. (2006) report that the most likely H-substitution mechanism in olivine is protonation of the O1-O2 edges of vacant M1 octahedra with a proton position at $x/a = 0.95$; $y/b = 0.04$; $z/c = 0.25$. Smyth et al. (2005) have measured the isothermal bulk moduli of a Fo₉₅ composition with about 8000 ppmw H₂O and report a bulk modulus of 120 GPa. It has the highest water concentration and lowest bulk modulus. In olivine, the important effects of hydrogen include a major decrease in strength in both the dislocation and diffusional creep regime (Mei and Kohlstedt 2000a, 2000b).

Raman scattering is a useful technique to study the interatomic forces and the local charge balance within the crystal structure. Kleppe et al. (2002, 2006) have studied the vibrational properties of the hydrous wadsleyite and hydrous γ -Mg₂SiO₄ using Raman spectroscopy. Raman studies and mode assignments for anhydrous forsterite and olivine with different compositions have been reported previously by Chopelas (1991), Iishi (1978), and Piriou and McMillan (1983); however, to our knowledge, Raman studies on hydrous forsterite and/or olivine have not yet been reported. Here, we report crystal structure and Raman spectroscopic data of synthesized hydrous forsterite by synchrotron X-ray diffraction and Raman scattering in a diamond anvil cell up to 41 GPa. Raman spectra of high-quality single crystals of hydrous forsterite were measured in the wide spectral range of 190–3700 cm⁻¹. Our aim was to investigate the effect of water on the vibrational properties and local structure of hydrous forsterite and to track changes in H bonding and proton environments under high pressure.

EXPERIMENTAL METHODS

Synthesis of hydrous forsterite

Synthesis of hydrous forsterite was carried out in double-capsule experiments in the 5000 ton multi-anvil press at Bayerisches Geoinstitut and described by Smyth et al. (2006). In these experiments, pyroxene-normative and periclase-normative compositions were formulated with about 3% by weight of H₂O. The two compositions were welded into separate inner Pt capsules and packed with brucite into a welded outer capsule. Crystalline phases were identified by Raman spectroscopy. The H contents were measured by polarized FTIR spectroscopy on

X-ray oriented, faceted single crystals. Table 1 lists the unit-cell parameters of the two hydrous forsterite samples SZ0408A and SZ0408B synthesized at 1250 °C and 12 GPa along with parameters for an anhydrous pure forsterite synthesized at 1600 °C and 1 atmosphere. Sample SZ0408A is pyroxene-normative, and forsterite coexists with clinoenstatite, whereas SZ0408B is periclase-normative, and forsterite coexists with hydroxyl-clinohumite.

The crystal size of sample SZ0408A was about 100–200 μm, whereas that of sample SZ0408B was less than 100 μm. The crystal size for the anhydrous sample was about 3 mm. In the two hydrous samples, H content was measured by polarized FTIR spectroscopy on X-ray oriented, faceted grains. The measured IR spectra are strongly pleochroic. Hydroxyl contents were computed from integrated absorbances using the calibration of Bell et al. (2003) for olivine. Representative polarized FTIR spectra from sample SZ0408A are given by Smyth et al. (2006).

Single-crystal X-ray diffraction

Unit-cell parameters (Table 1) were measured using Bruker P4 four-circle X-ray single-crystal diffractometer equipped with a point detector and mounted on an 18-kw rotating anode X-ray generator (Smyth et al. 2006). Single-crystal X-ray intensity data were measured on a Bruker APEX II CCD detector system and also on a Bruker P4 diffractometer on the rotating anode source. For sample SZ0408A and the anhydrous sample, intensities were measured out to about 100 °2θ, but in the smaller SZ0408B crystal, intensity measurements were not made beyond 80°. Structure refinements were carried out with the SHELXL-97 program package (Sheldrick 1997). Scattering factors used in refinements were those of Cromer and Mann (1968) for Mg²⁺ and Si⁴⁺. A mixed scattering was used for oxygen with 20% O⁻¹ (Cromer and Mann 1968) and 80% O⁻² (Tokonami 1965). With oxygen sites fixed at full occupancy, this method gives full unconstrained occupancies for all cation sites in the anhydrous sample. Refinement parameters are given in Table 1, and final position and displacement parameters in Table 2. Nearest neighbor distances and coordination polyhedron parameters were calculated using the package METRIC (Bartelmehs et al. 1993) and are reported in Table 3.

Refined occupancy parameters (Table 2) show full occupancy in both octahedral and tetrahedral sites in the anhydrous sample, but less than full occupancy in the M1 and the Si site in both of the hydrous samples. The M2 site appears to show near full occupancy on all samples. Polyhedral volumes (Table 3) indicate expansion of both M1 and M2 relative to the anhydrous sample, but little or no expansion of the tetrahedral site. Occupancy refinements are very sensitive to positional disorder, and the refinements of hydrous samples all show atomic displacement parameters about 20% larger than those of the anhydrous sample.

Raman spectroscopy

Raman scattering experiments were conducted by use of Dilor XY micro-Raman system, with the spectrometer equipped with a liquid nitrogen-cooled charge-coupled-device (CCD) detector. A randomly oriented single-crystal fragment from the specimen, approximately 30 × 35 × 20 μm thick, was selected and placed in an 85 μm diameter hole of pre-indented rhenium gasket (40 μm thick) in a diamond cell with 350 μm size culets. The specimen was excited by the 514.5 nm green line of Spectra Physics Ar ion laser. Three small pieces of ruby (~3 μm in size) were placed around the specimen for pressure calibration. Liquid argon was loaded as a pressure-transmitting medium using the liquid nitrogen loading technique. The laser light was focused on the specimen to about a 5 μm diameter spot with a power of 15 mW. A 50× objective was used to focus the incident laser light on the specimen and also to collect the scattered light. No laser heating effects were observed. The spectrometer was calibrated using single-crystal silicon as a

TABLE 1. Structure refinement and unit-cell parameters of anhydrous and hydrous forsterite

Parameter	Anhydrous	Hydrous	
		SZ0408A	SZ0408B
<i>a</i> (Å)	4.7552(2)	4.7545(4)	4.7547(4)
<i>b</i> (Å)	10.1985(2)	10.2068(8)	10.20416(8)
<i>c</i> (Å)	5.9822(2)	5.9863(4)	5.98494(4)
<i>V</i> (Å ³)	290.11(2)	290.50(3)	290.373(3)
2θ max (°)	100	100	80
No. meas.	7145	8665	4385
No. unique	1110	1277	972
No. unique > 4σ	1051	1181	804
<i>R</i> _{int}	0.026	0.026	0.027
<i>R</i> > 4σ	0.019	0.021	0.032

TABLE 2. Fractional atomic coordinates, occupancy, and displacement parameters for anhydrous and hydrous forsterite

Atom	<i>x/a</i>	<i>y/b</i>	<i>z/c</i>	Occ.*	<i>U</i> ₁₁	<i>U</i> ₂₂	<i>U</i> ₃₃	<i>U</i> ₁₂	<i>U</i> ₁₃	<i>U</i> ₂₃	<i>U</i> _{eq}	Site Pot. (V)
Anhydrous Fo100												
Mg1	0.0	0.0	0.0	0.997(3)	0.0060(1)	0.0080(1)	0.0056(1)	0.0	0.0	0.0	0.00651(8)	-23.477
Mg2	0.99148(7)	0.27747(3)	0.25	0.999(3)	0.0067(1)	0.0056(1)	0.0066(1)	0.0	0.0	0.00015(9)	0.00629(8)	-25.132
Si1	0.42643(5)	0.09402(2)	0.25	0.995(3)	0.0040(1)	0.0048(1)	0.0049(1)	0.0	0.0	0.00004(6)	0.00456(7)	-46.834
O1	0.7660(1)	0.09150(6)	0.25	1.0	0.0039(2)	0.0069(2)	0.0063(2)	0.0	0.0	0.0001(2)	0.0057(1)	27.672
O2	0.2217(1)	0.44710(6)	0.25	1.0	0.0056(2)	0.0047(2)	0.0064(2)	0.0	0.0	-0.0000(2)	0.0056(1)	27.511
O3	0.2775(1)	0.16305(4)	0.03313(8)	1.0	0.0057(2)	0.0069(2)	0.0056(2)	0.0014(1)	-0.0003(1)	0.0002(1)	0.00606(9)	26.341
SZ0408A												
Mg1	0.0	0.0	0.0	0.984(2)	0.0064(1)	0.0090(1)	0.00638(9)	0.0	0.0	0.0	0.00728(7)	-23.464
Mg2	0.99130(7)	0.27702(3)	0.25	1.002(2)	0.0073(1)	0.00638(9)	0.0081(1)	0.0	0.0	0.00028(8)	0.00725(7)	-25.144
Si	0.42626(5)	0.09377(2)	0.25	0.994(2)	0.00425(9)	0.00561(9)	0.00558(9)	0.0	0.0	0.00004(6)	0.00515(6)	-46.736
O1	0.7661(1)	0.09134(6)	0.25	1.0	0.0042(2)	0.0074(2)	0.0062(2)	0.0	0.0	-0.0001(2)	0.00593(9)	27.668
O2	0.2217(1)	0.44673(6)	0.25	1.0	0.0063(2)	0.0057(2)	0.0072(2)	0.0	0.0	-0.0004(2)	0.00640(9)	27.497
O3	0.27705(9)	0.16301(4)	0.03280(7)	1.0	0.0061(1)	0.0073(1)	0.0064(1)	0.0011(1)	0.0001(1)	-0.0000(1)	0.00662(8)	26.292
SZ0408B												
Mg1	0.0	0.0	0.0	0.990(4)	0.0065(3)	0.0089(3)	0.0070(2)	0.0	0.0	0.0	0.0075(2)	-23.459
Mg2	0.9911(2)	0.27714(7)	0.25	1.001(2)	0.0074(3)	0.0070(2)	0.0090(3)	0.0	0.0	0.0000(2)	0.0078(2)	-25.144
Si	0.4263(1)	0.09380(5)	0.25	0.993(2)	0.0047(2)	0.0061(5)	0.0073(9)	0.0	0.0	0.0002(2)	0.0060(1)	-46.798
O1	0.7659(3)	0.0914(1)	0.25	1.0	0.0047(6)	0.0072(5)	0.0076(5)	0.0	0.0	0.0006(4)	0.0065(2)	27.685
O2	0.2216(3)	0.4469(1)	0.25	1.0	0.0067(6)	0.0063(5)	0.0079(5)	0.0	0.0	-0.0005(4)	0.0070(2)	27.474
O3	0.2774(2)	0.16284(9)	0.0330(2)	1.0	0.0066(4)	0.0073(4)	0.0082(6)	0.0012(3)	-0.0003(3)	0.0005(3)	0.0074(2)	26.333

TABLE 3. Coordination polyhedra for anhydrous and hydrous forsterite

	Anhydrous	Hydrous	
		SZ0408A	SZ0408B
Si tetrahedron			
Si-O1	1.6149(7)	1.6161(6)	1.615(2)
Si-O2	1.6556(7)	1.6575(6)	1.656(1)
Si-O3(2)	1.6373(5)	1.6411(4)	1.638(1)
<Si-O>	1.6362(6)	1.6390(5)	1.637(1)
TQE	1.0112	1.0110	1.0110
PolyVol	2.211(1)	2.223(1)	2.214(2)
M1 octahedron			
Mg-O1(2)	2.0846(5)	2.0846(4)	2.085(1)
Mg-O2(2)	2.0687(4)	2.0702(4)	2.070(1)
Mg-O3(2)	2.1319(5)	2.1312(4)	2.131(1)
<Mg-O>	2.0961(5)	2.0953(4)	2.095(1)
OQE	1.0269	1.0263	1.0267
PolyVol	11.785(2)	11.799(2)	11.792(4)
M2 octahedron			
Mg-O1(1)	2.1787(7)	2.1767(7)	2.177(2)
Mg-O2(1)	2.0471(7)	2.0496(7)	2.050(2)
Mg-O3(2)	2.2122(5)	2.2114(5)	2.214(1)
Mg-O3(2)	2.0670(5)	2.0684(5)	2.068(1)
<Mg-O>	2.1307(6)	2.1310(6)	2.132(1)
OQE	1.0262	1.0257	1.0260
PolyVol	12.428(2)	12.441(2)	12.446(4)

reference. The pressure was estimated using the shift in the R1 line of the ruby loaded along with the specimen. All spectra were recorded in the backscattering geometry with no polarization used for the collected signal.

RESULTS AND DISCUSSION

Crystal lattice and vibrational modes in hydrous forsterite at ambient pressure

The olivine (forsterite) structure is orthorhombic containing isolated SiO₄ units linked by octahedrally coordinated Mg²⁺ cations as shown in Figure 1. The cations are in two crystallographically distinct sites, the smaller M1 (*C_i* symmetry) site and larger M2 (*C_s* symmetry) site. The M1 octahedron shares six edges with neighboring polyhedra and two with SiO₄ tetrahedra. The M2 octahedra share three edges with neighboring polyhedra, but only one with a SiO₄ tetrahedron.

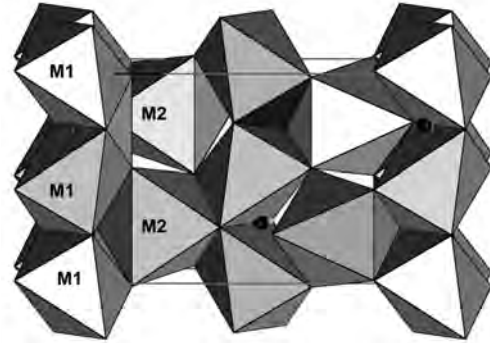


FIGURE 1. Crystal structure of olivine; *c*-axis is vertical; *b*-axis is horizontal. The M1 octahedron lies at the origin of the unit cell (outlined), whereas the M2 octahedron and Si tetrahedron lie on the mirror plane normal to the *c*-axis. The proton (dark sphere) on the O1-O2 shared edge of the M1 octahedron is illustrated.

Before performing the high-pressure Raman measurements, we examined the optical phonons and phonon dispersion in hydrous forsterite at ambient conditions. The notations in Figure 2 are as follows: 1a, 2a, 1b, 2b represent the measured spectra in different orientations by tilting the sample less than 10° and rotating 90°. Our results show that the dispersion of the Raman modes in hydrous forsterite is small, especially of the two high-frequency *A_g* modes at 824.4 and 856.2 cm⁻¹. Our ambient Raman frequencies agree very well with those reported in previous studies (Iishi 1978; Piriou and McMillan 1983; Gillet et al. 1991; Chopelas 1990, 1991; Durben et al. 1993; Wang et al. 1993). From the greater extent of edge sharing between SiO₄ and M1O₆ polyhedra, one might expect the M1 cation to have a greater influence on the SiO₄ internal mode frequency. Interestingly, we did not observe significant effects of the water on the Raman mode frequencies in hydrous forsterite (SZ0408A) as compared to the previously reported data for anhydrous forsterite. Figure 3 shows the ambient pressure unpolarized Raman spectra of hydrous forsterite (SZ0408A) and pressure-quenched (from 41 GPa) hydrous forsterite in the OH-stretching region (3400–3700 cm⁻¹).

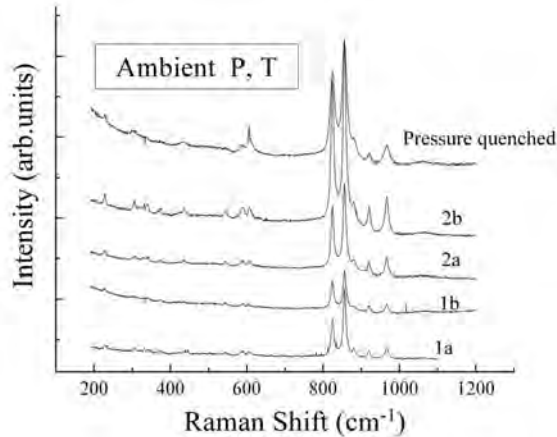


FIGURE 2. Raman spectra of hydrous forsterite (SZ0408A, as received) at ambient pressure. Spectra 1a, 1b, 2a, and 2b were taken on this specimen in slightly different orientations. Also shown is the spectrum of this specimen at ambient pressure after it was pressurized to ~41 GPa and quenched (see text).

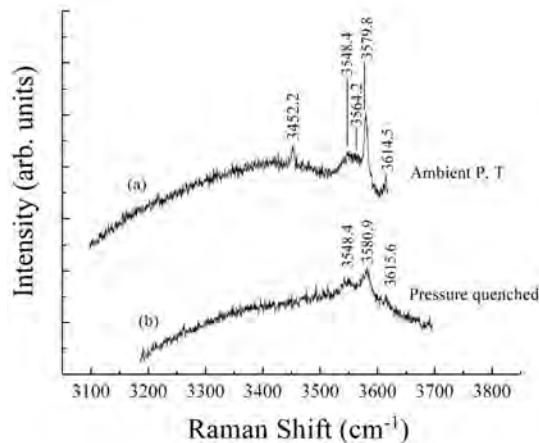


FIGURE 3. Ambient Raman spectra of hydrous forsterite (SZ0408A) in the OH-stretching region (3100–3700 cm^{-1}). (a) Spectrum is obtained from the sample “as received”. (b) Spectrum is the sample pressure-quenched from 41 GPa.

The upper spectrum (Fig. 3a) shows five Raman bands observed at 3452, 3548, 3564, 3580, and 3615 cm^{-1} ; these frequencies are similar to the FTIR spectra (within 2–3 cm^{-1}) measured on the same sample (Smyth et al. 2006). The lower spectrum (Fig. 3b) obtained from the pressure-quenched sample has only 3 bands, and the OH band that was observed at ambient pressure (Fig. 3a) at 3452 cm^{-1} is not observed. The three modes show some broadening as compared to the modes measured at ambient pressure. The detailed pressure dependencies of hydroxyl group vibrations are discussed in below. (Pressure dependencies of O-H-stretching modes in hydrous forsterite.)

Raman spectra at high pressure

Figure 4 shows Raman spectra of hydrous forsterite (SZ0408A) in the range of 190–1200 cm^{-1} up to 41 GPa. The lattice vibrational modes, observed in the lower-frequency range (200–750 cm^{-1}) and the SiO_4 internal modes in the higher-

frequency range (800–1200 cm^{-1}) are presented separately. Data analysis of the spectra was carried out using ORIGIN Pro 7.5 software with Lorentzian function. The obtained frequencies, full-width at half maximum (FWHM), and normalized intensity of the two A_g modes (824.4 and 856 cm^{-1}) are shown in Table 4. Intensity of these two A_g modes are normalized to the sum of the intensity of the high-frequency Raman modes between 800 and 1100 cm^{-1} . The frequencies of all the observed modes are plotted as a function of pressure in Figures 5 and 6. It is evident in Figures 5 and 6 that: (1) the frequencies of all the modes increase linearly with increasing pressure throughout the pressure range (the derivatives are given in the parentheses), and (2) at ~20 GPa, there are marked changes (decreases) in the pressure derivatives of both the lattice modes and the SiO_4 internal stretching vibrational modes. In contrast, previous Raman studies on anhydrous forsterite have not reported such a slope change at ~20 GPa. However, Durben et al. (1993) reported new bands near 750 and 950 cm^{-1} , an increasing intensity of the band in the 600–800 cm^{-1} region, and a subtle kink in the trend of pressure dependencies of many of the observed Raman bands in anhydrous forsterite near ~30 GPa. They interpreted these changes as evidence of the appearance of defect structures through the formation of Si-O-Si linkages accompanied by an increase in the silicon coordination. However, our spectra did not show such a feature, indicating that hydrous forsterite remains characteristic of an orthosilicate structure up to the studied pressure range in this study. Van de Moortèle et al. (2007) observed that shocked

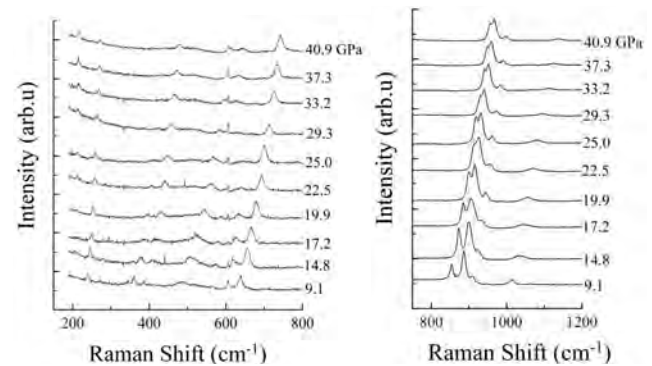


FIGURE 4. Raman spectra of hydrous forsterite (SZ0408A) to 40.9 GPa in two frequency ranges (200–800 and 800–1200 cm^{-1}).

TABLE 4. Frequencies, full-width at half maximum (FWHM), normalized intensity, and intensity ratio of the two A_g modes (824.4 and 856 cm^{-1}) of hydrous forsterite (SZ0408A)

Pressure (GPa)	Frequency (cm^{-1})	FWHM (cm^{-1})	$I_{\text{nor}1}$	Frequency (cm^{-1})	FWHM (cm^{-1})	$I_{\text{nor}2}$	I_2/I_1
1.00E-04	824.4	9.3(1)	0.352	856.2	9.4(1)	0.466	1.325
6.4	846.3	9.7(1)	0.309	878.8	9.6(1)	0.534	1.729
9.1	854.1	11.0(2)	0.243	886.7	11.9(1)	0.555	2.279
11.9	862.6	9.4(2)	0.241	893.3	15.7(1)	0.598	2.482
14.8	874.1	9.5(2)	0.218	900.7	22.0(3)	0.642	2.939
17.2	884.6	9.6(3)	0.189	906.5	22.4(4)	0.652	3.442
19.7	900.4	9.4(3)	0.208	914.9	18.1(2)	0.621	2.979
22.5	913.1	11.4(4)	0.224	926.2	16.8(4)	0.566	2.528
25	918.2	11.1(2)	0.303	932.1	13.7(2)	0.486	1.603
29.3	929.6	11.2(3)	0.263	940.9	13.0(2)	0.505	1.920
33.2	941.0	9.8(2)	0.267	952.4	12.7(2)	0.541	2.026
37.3	948.3	10.2(3)	0.259	960.1	13.6(3)	0.555	2.140
40.9	955.6	10.0(3)	0.258	967.4	13.6(3)	0.566	2.188

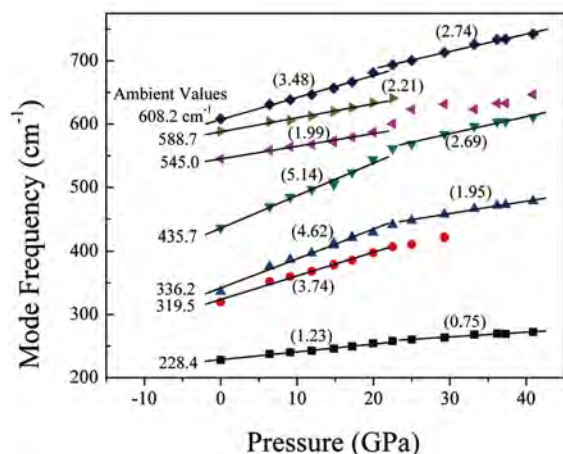


FIGURE 5. Pressure dependencies of the observed low-frequency lattice vibrational modes in the 200–750 cm^{-1} range; pressure derivatives are given in parentheses.

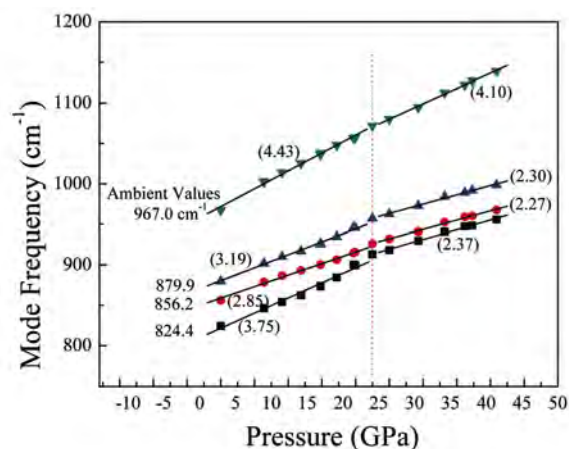


FIGURE 6. Pressure dependencies of four high-frequency SiO_4 internal stretching vibrational modes in the 800–1200 cm^{-1} range; pressure derivatives are given in parentheses.

olivines give rise to a new orthosilicate polymorph that is formed metastably during the shock process and that is subsequently recovered to ambient conditions. The slope change at 20 GPa in our study may be related to such structural modification in hydrous forsterite. In this study, the Raman mode frequencies of the O-H groups also show a change in the $(\partial v_i/\partial P)$ slope around 20 GPa, accompanied by the appearance of a new peak (see below). The changes in O-H modes at the same pressure range with SiO_4 modes and M modes may imply the structural modification in hydrous forsterite, closely related to the proton dynamics in the crystal at high pressure.

The high-frequency Raman modes in olivine represent the stretching vibrations of the SiO_4 tetrahedra (Piriou and McMillan 1983; Lam et al. 1990). For an isolated SiO_4 tetrahedron, there are four types of symmetry modes: ν_1 , ν_2 , ν_3 , and ν_4 . Usually, it is assumed that the tetrahedral vibrations are independent internal modes in olivines, as observed in isotopic exchange experiments (Paques-Ledent and Tarte 1973; Piriou and McMillan 1983). The highest-frequency A_g mode observed at 967.0 cm^{-1} at ambient

pressure is mainly the Si-O1 stretch of ν_3 symmetry type. The second highest frequency A_g mode at 856.2 cm^{-1} is predominantly Si-O3(O4) vibration; and the A_g mode at 824.4 cm^{-1} is mainly the Si-O2 stretch. These two modes have a significant mixing of ν_3 and ν_1 character. The A_g mode at 824.4 cm^{-1} has more ν_3 character, whereas the second highest frequency A_g mode at 856.2 cm^{-1} has more ν_1 character. The B_{2g} mode observed at 879.9 cm^{-1} at ambient pressure has the ν_3 character. The frequencies of the three A_g modes increase linearly with pressure, and clearly show decrease in the $(\partial v_i/\partial P)$ slopes at ~ 22.5 GPa as shown in Figure 6. The mode at 967.0 cm^{-1} shows the highest pressure dependence among the three high-frequency A_g modes of SiO_4 tetrahedra, in agreement with Chopelas (1991). The Si-O1 bond is the shortest (1.61 vs. 1.66 and 1.65 Å) among the other Si-O bonds. Lam et al. (1990) pointed out that there is a net force on the Si toward O1 resulting from the Coulomb repulsion between Si and the three basal magnesium atoms. The force on Si is responsible for making the Si-O1 distance shorter than the other Si-O distances, and makes the mode at 977.0 cm^{-1} sensitive to the volume of the M1 and M2 octahedra. Such volume dependence of this mode (977.0 cm^{-1}) is consistent with the symmetry analysis for olivines and orthosilicates (Paques-Ledent and Tarte 1973; Piriou and McMillan 1983). Piriou and McMillan (1983) have discussed such volume dependence of high-frequency A_g modes of SiO_4 tetrahedra in response to Ca^{2+} substitutions in the M sites, and found that asymmetric stretching ν_3 mode has stronger volume dependence as compared to symmetric stretching mode ν_1 . These authors used a model of two coupled harmonic oscillators to discuss the mixing and crossover behavior of the two high-frequency A_g modes (824.4 and 856.2 cm^{-1}), and proposed the degree of coupling should increase through tephroite and monticellite to forsterite. Referring to Figure 7, we observe that the ratio of the integrated intensity of the two high-frequency A_g modes (824.4 and 856.2 cm^{-1}) increases and then decreases sharply, indicating strong coupling between these two modes as discussed below. At higher pressures SiO_4 tetrahedral vibrations are no longer independent internal modes in forsterite.

Using the concept of a model of two coupled harmonic oscillators, (Piriou and McMillan 1983) have shown that the Raman

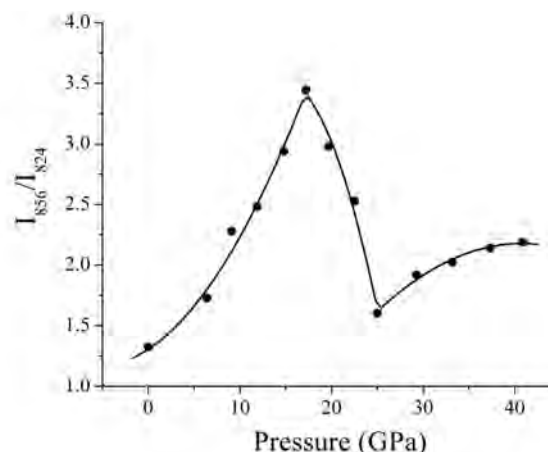


FIGURE 7. Pressure dependence ratio of the integrated intensity of the two high-frequency Raman modes (824.4 and 856.2 cm^{-1}) vs. pressure.

intensity of the two A_g modes is related to their proportion of v_1 character. Thus as seen in Figure 7, a steep intensity transfer between the two modes (824.4 and 856.2 cm^{-1}) appears to occur with increasing pressure, indicating that these two vibrations are weakly coupled at ambient pressure, whereas the coupling is enhanced at higher pressure. A crossover takes place between these two modes, which implies that the ionic motions associated with the two-phonon modes are transferred to each other. In this pressure range (0–17.5 GPa), the inter-tetrahedral O-O force increases with pressure (Lam et al. 1990). In the pressure range 0–17.5 GPa, the ratio of integrated intensity increases as expected, and the A_g mode at 824.4 cm^{-1} has more v_3 character showing higher compressibility than the A_g mode at 856.2 cm^{-1} , which has more v_1 character. However, between 17.5 and 25 GPa, there must be some other mechanism to account for the decrease in the intensity ratio with increasing pressure. All the spectra in the diamond anvil cell were taken in nearly the same geometry (orientation), and the changes in the intensity of two A_g modes are not from the effect of sample orientation. The spectral analysis was carried out using a Lorentzian spectral function. In this case, the integrated intensity of a Raman mode is equal to the oscillator strength in the damped harmonic oscillator model. In this model, oscillator strength is related to the reduced mass of the oscillator and the effective charge. Considering the hydrogen influence in hydrous forsterite, the effect on the reduced mass of the oscillator should be smaller than the effect on the effective charge of the oscillator. Our results (Fig. 7) suggest that the effect of hydrogen on the effective charge is significant for the two modes at 824.4 and 856.2 cm^{-1} . It is interesting to note that the OH mode at 3580 cm^{-1} disappears above 13 GPa; this is attributed to the positional ordering of hydrogen between Si-O2 and Si-O3(O4) sites.

Using the observed pressure derivatives of the Raman frequency modes, $(\partial v_i / \partial P)$, the mode Grüneisen parameters, γ_i , were calculated from $\gamma_i = (K_T / v_{i0}) (\partial v_i / \partial P)_T$ (see Table 5). Figure 8 shows calculated mode Grüneisen parameters (γ_i) of hydrous forsterite (SZ0408A) plotted as a function of frequency. As can be seen, mode γ_i values related to $\text{Mg}(2)\text{O}_6$ translation and SiO_4

rotation have higher values than those of SiO_4 internal modes. This is consistent with higher compressibility of the $\text{Mg}(2)\text{O}_6$ octahedra as compared to SiO_4 tetrahedra. To examine the effects of hydration on γ_i , we have plotted the relative changes of γ_i , defined as $(\gamma_i^{\text{hydrous}} - \gamma_i^{\text{anhydrous}}) / \gamma_i^{\text{anhydrous}}$ for hydrous forsterite (see Fig. 9). Note the mode γ_i 's related $\text{Mg}(2)\text{O}_6$ translation and SiO_4 tetrahedra modes show significant differences in hydrous forsterite (SZ0408A) as compared to those in anhydrous forsterite (Chopelas 1991). Mode γ_i 's related to $\text{Mg}(2)\text{O}_6$ translation are lower in hydrous forsterite as compared to those in anhydrous forsterite. This difference may be attributed to the full occupancy of M2 site as compared to M1 site, and the existence of the vacancy at M1 site in hydrous forsterite (SZ0408A). The mode γ_i values related to SiO_4 tetrahedra have divergent values. For example, γ_i values of the A_g mode at 856.2 cm^{-1} (mainly Si-O3 stretch) and the A_g mode at 967.0 cm^{-1} (mainly Si-O1 stretch) are smaller in hydrous forsterite, while γ_i value of the A_g mode at 824.4 cm^{-1}

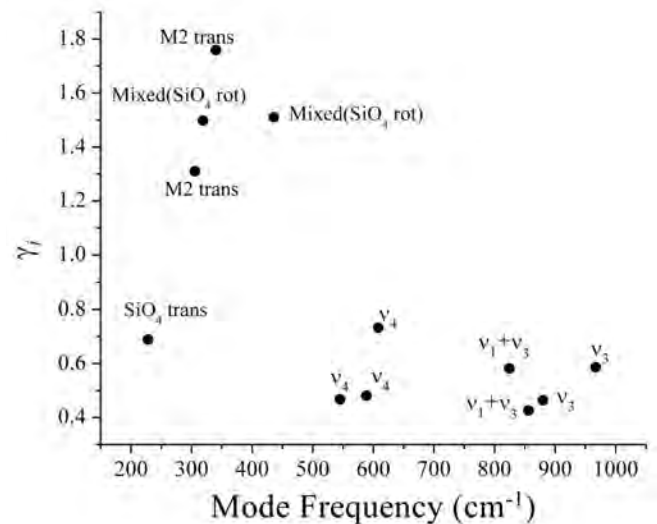


FIGURE 8. Mode Grüneisen parameters, γ_i , for various frequency modes.

TABLE 5. Mode frequencies (in cm^{-1}), mode Grüneisen parameters, and mode assignments for vibrational modes of hydrous forsterite and anhydrous forsterite (Chopelas 1991)

Symmetry	This study		Chopelas (1991)			Mode type
	Mode frequency	Mode Grüneisen parameter	Mode frequency randomly oriented	Mode frequency oriented single crystal	Mode Grüneisen parameter	
A_g	228.4	0.689(28)	227	226	0.674	SiO_4 translation
	248.1		244	242	1.21	
A_g	305.6	1.31(12)	306	304	1.63	M2 translation
	319	1.498(68)				
B_{1g}	331.2		331	329	1.16	SiO_4 rotation
A_g	340.2	1.759(68)	341	339	1.87	M2 translation
B_{3g}	373.1		376	374	1.25	Mix(M2 Trans)
			411	410	0.99	
			424	422	1.43	v_2
B_{3g}	435.7	1.51(7)	434	435	1.4	Mix (SiO_4 rotation)
B_{2g}			441		1.6	v_2
A_g	545	0.467(23)	545	545	0.528	v_4
B_{2g}			585	586	0.659	
B_{3g}	588.7	0.481(19)		592		v_4
A_g	608.2	0.732(32)	609	608	0.704	v_4
A_g	824.4	0.582(26)	826	824	0.483	v_1+v_3
A_g	856.2	0.426(12)	856	856	0.489	v_1+v_3
B_{2g}	880	0.464(13)	884	881	0.439	v_3
B_{3g}	921		922	920	0.382	v_3
A_g	967	0.586(20)	966	965	0.661	v_3

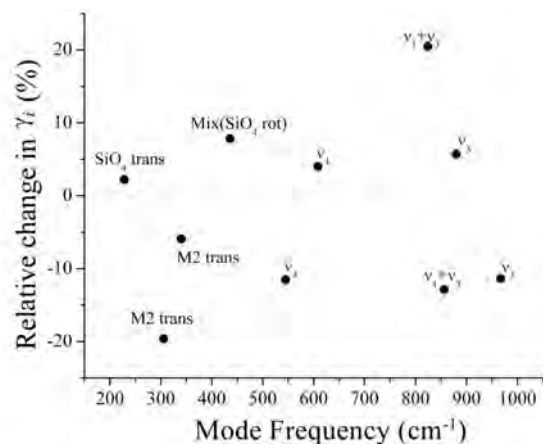


FIGURE 9. Relative changes of γ_i in hydrous forsterite (SZ0408A) as compared to anhydrous forsterite; here, relative changes are defined as $(\gamma_{i \text{ hydrous}} - \gamma_{i \text{ anhydrous}})/\gamma_{i \text{ anhydrous}}$.

(mainly Si-O2 stretch) is larger. One possible explanation for this is that local charge balance results in an increase of γ_i of the Si-O2 stretch mode, implying higher compressibility of this stretch mode. In hydrous forsterite, all O atoms are bonded to three Mg and one Si atoms. The major H substitution mechanism in olivine is protonation of the O1-O2 edges of vacant M1 octahedra (Smyth et al. 2006). The single-crystal XRD data suggest that the proton is closer to O2 than O1, the distance between the proton and O2 being 0.96 Å.

The pressure dependencies of O-H-stretching modes in hydrous forsterite

The Raman modes of hydroxyl groups in hydrous forsterite (SZ0408A) are shown in Figure 10. The observed spectra from ambient pressure to 13 GPa have been fitted into five Gaussian functions using ORIGIN Pro 7.5. The spectra above 13 GPa are fitted with three Gaussian functions (Fig. 11). The pressure dependencies of the five OH-stretching frequencies show nonlinear and somewhat complex behavior, as shown in Figure 12. For the four modes at 3615, 3580, 3564, and 3548 cm^{-1} , the frequency slightly decreases with increasing pressure (up to ~10 GPa): the $(\partial\nu/\partial P)$ slopes approximately are -0.43 , -1.4 , -0.64 , and -0.36 , respectively. The negative pressure dependence indicates strengthening of hydrogen bonding at higher pressures (up to ~10 GPa). The 3615 cm^{-1} OH mode initially decreases with increasing pressure, reaches a minimum at around 6.4 GPa, increases up to 20 GPa, and then did not show marked pressure dependencies. The $(\partial\nu/\partial P)$ slope changes from -0.43 below 10 GPa to 1.97 between 10 and 20 GPa. Generally, with increasing pressure, interatomic distance becomes shorter, and the strength of hydrogen bonding increases monotonously. In the present study, however, the strength of hydrogen bonding at 3615 cm^{-1} indicates complex responses to pressure. The peak is strongly polarized in the a -direction (Smyth et al. 2006). In addition to the mode frequency, the intensity of the observed OH modes also changes with increasing pressure. The 3580 cm^{-1} mode is broadened with increasing pressure, and disappears above 13 GPa. The intensity of the 3615 cm^{-1} mode increases with pressure, and remains constant above 20 GPa, and a new peak (3503 cm^{-1}) appears at ~20 GPa. These results show that some

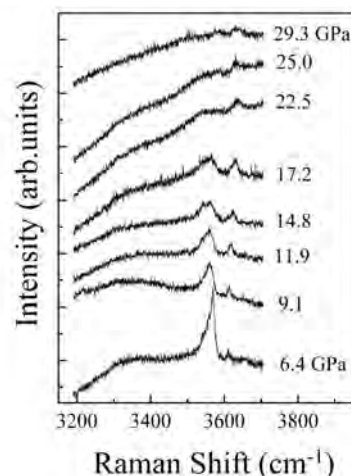


FIGURE 10. Raman spectra of hydrous forsterite (SZ0408A) in the OH-stretching region up to 29.3 GPa.

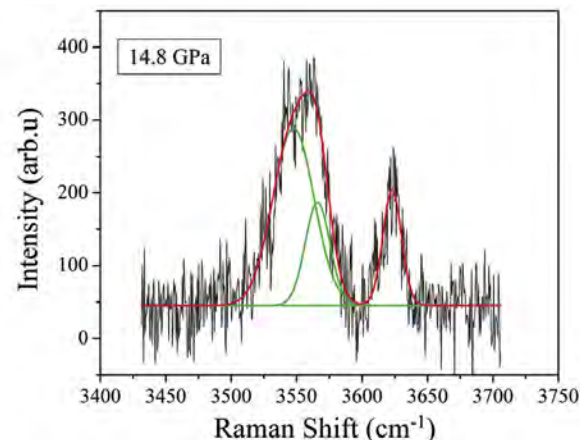
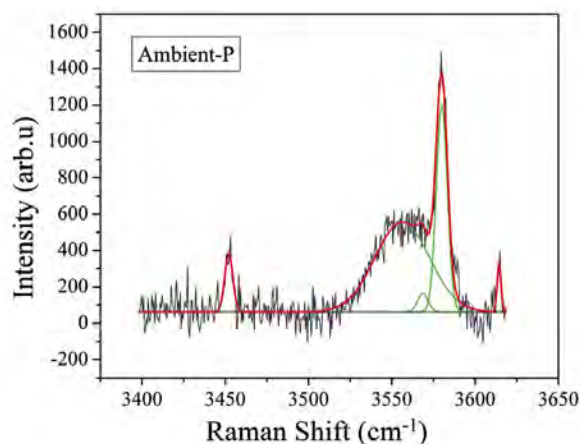


FIGURE 11. Examples of fitting of the Raman spectra of hydrous forsterite in the OH region at ambient pressure and 14.8 GPa.

exchange of H between sites occurs. Previous studies (Bai and Kohlstedt 1993; Kohlstedt et al. 1996; Matveev et al. 2001; Walker et al. 2007; Litasov et al. 2007) indeed have reported that there are two different mechanisms related to silicon and magnesium vacancies by which hydrogen is incorporated into

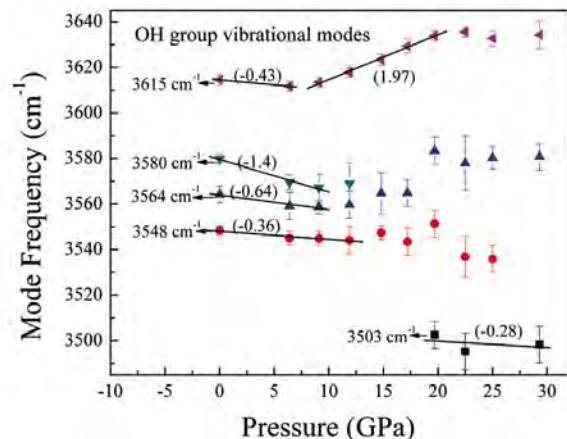


FIGURE 12. Pressure dependencies of four OH-stretching modes (3548, 3564, 3580, and 3615 cm^{-1}) in hydrous forsterite. The initial negative pressure derivatives for these four OH-stretching modes up to ~ 10 GPa and the positive pressure derivatives for the 3615 cm^{-1} OH mode in the pressure range of 10–20 GPa are given in parentheses. Also shown are the data for the 3503 cm^{-1} mode.

olivine crystal structure. Our results (Fig. 12) suggest that proton ordering is likely to occur between the octahedral and tetrahedral sides in olivine.

OH-stretching frequencies and O \cdots O distances

Unit-cell parameters and preliminary occupancy refinements for two hydrous forsterite samples were reported by Smyth et al. (2006). Preliminary intensity data collections were performed for that study on a point-detector diffractometer with maximum 2θ of 75° . For the current refinements, data were collected to a maximum two-theta of 80 to 100° (Table 1) using a Bruker APEX II CCD detector giving redundancy of equivalent reflection intensity measurements of four to eight times those of the point detector data sets (Table 1). Occupancy refinements are sensitive to the scattering models used for the cations and O atoms and somewhat sensitive to the high-angle reflection intensities. In the current study (Tables 2 and 3), occupancy and atom position refinement precisions are improved over the preliminary study by factors of three to five. We have also refined the structure of an anhydrous forsterite with a similar procedure for direct comparison.

In the structure details (Table 3), we observe significant expansion of both the M1 and M2 coordination polyhedral primarily due to elongation of the Mg1-O2 and Mg2-O2 distances. The protonation of olivine has been studied extensively by FTIR spectroscopy. Previous studies show that there are two different mechanisms related to silicon and magnesium vacancies by which hydrogen is incorporated into the olivine crystal structure. Bai and Kohlstedt (1993) and Kohlstedt et al. (1996) suggested protonation of Mg-vacancies in the olivine structure, while Matveev et al. (2001) and Lemaire et al. (2004) preferred significant protonation of Si-vacancies. The FTIR spectra of hydrous forsterite (SZ0408A) show five absorbance peaks at 3612, 3578, 3552, and 3566 cm^{-1} . The E//a spectra show strong absorbance peaks at 3612 and 3578 cm^{-1} ; E//b has a sharp feature 3578 and much broader peak at 3552 cm^{-1} ; and E//c at 3566

cm^{-1} (Smyth et al. 2006). Strong absorbance in this frequency range is consistent with protonation of the octahedral edges (Libowitzky 1999). Octahedral edges in the olivine structure range from 2.85 to 3.33 \AA except for the edge shared with the tetrahedron, which is about 2.55 \AA . Tetrahedral edges range from 2.55 to 2.76 \AA . So, the strong absorbance features of these spectra are more consistent with protonation of the octahedral edges than of the tetrahedral edges. The largest peak in the pattern is at 3612 cm^{-1} and is strongly polarized in the *a*-direction. This frequency corresponds to protonation of an O-O distance of >2.8 \AA (Libowitzky 1999), and is consistent with the O1-O2 edge shared between M1 octahedra (2.85 \AA). This would place the proton at about 1.0 \AA from either O1 or O2. Smyth et al. (2006) suggested a proton position on O1. From the interatomic distances presented in Table 3, it appears that the major difference between the hydrous and anhydrous samples is the expansion of distances around O2. This would imply that the proton is closer to O2 than O1. Proton coordinates that would satisfy this would be $x/a = 0.09$; $y/b = 0.98$; $z/c = 0.25$. This would give a proton to O2 distance of 0.96 \AA and a very strong polarization in the *a*-direction. This position is shown in Figure 1.

According to the empirical relation between OH-stretching frequencies and O \cdots O distances (Libowitzky 1999), a negative frequency response of OH modes under pressure requires a reduction of the respective O \cdots O distances and indicates a strengthening of the hydrogen bond. A negative frequency response of OH mode at 3615 cm^{-1} under pressure (below 10 GPa) implies shortening of this O1-O2 octahedral edge and reflects strengthening of the hydrogen bond. However, above 10 GPa, the respective O1-O2 distance increases and the hydrogen bond is weakening. As pressure increases further, the OH mode at 3615 cm^{-1} does not show clear pressure dependence. A nearly constant OH mode frequency suggests very weak hydrogen bonding in O1-O2 octahedral edge at pressures above 20 GPa.

Negative pressure dependencies of OH-stretching frequencies are common and better understood than positive pressure dependencies (Kleppe and Jephcoat 2006). Kleppe et al. (2006) observed negative or nearly constant pressure dependencies of the OH-stretching modes in hydrous wadsleyite. The positive pressure dependence of the OH-stretching mode at 3617 cm^{-1} are reported using Raman spectroscopy, and attributed to the very weak or absent hydrogen bonds in the Phase E (Kleppe et al. 2001). Extensive positive pressure dependence of OH bands in coesite have been reported and interpreted as an increase of the corresponding O-H \cdots O distances with pressure (Koch-Müller et al. 2003). Contrary to the other dense hydrous magnesium silicates, positive pressure dependencies were also observed for chondrodite and clinohumite (Lin et al. 1999, 2000). They were explained as being due to a combination of H-H repulsion and hydrogen-bond elongation toward an empty polyhedron. In our case, the positive pressure dependence of the OH-stretching mode at 3615 cm^{-1} above 10 GPa is not likely originated from the H-H repulsion. An alternative interpretation for the positive pressure dependence above 10 GPa is the possibility of the changes from hydrogen-bonded OH-stretching mode to a non-hydrogen bonded mode. In the case of non-hydrogen bonds, the OH-stretching frequency is expected to increase with pressure in accord with compression of the OH bond, as in case of the

other lattice modes.

These results are a part of systematic investigation of the effects of hydration, pressure, and temperature on the physical properties of mantle minerals. It is clear that H is the most significant compositional variable that can affect these properties, and may exceed temperature effects on velocity heterogeneity in the upper mantle. To assess the H content of the upper mantle, it will be necessary to place tighter constraints on the pressure and temperature derivatives of the elastic parameters of hydrous phases. Raman spectroscopy of the hydrous mantle phases, under in situ high-*P/T* conditions, also holds promise for elucidating their stability.

ACKNOWLEDGMENTS

We are grateful to John Balogh (University of Hawaii) for maintaining high pressure spectroscopy facility, and to Diane Henderson for editorial help in improving the manuscript. This work was supported by U.S. National Science Foundation Grants EAR 05-38884 to M.H. Manghni and EAR 07-11165 to J.R. Smyth, and the Bayerisches Geoinstitut Visitors Program, SOEST and Hawaii Institute of Geophysics and Planetology contribution no. 7557.

REFERENCES CITED

- Bai, Q. and Kohlstedt, D.L. (1993) Effects of chemical environment on the solubility and incorporation mechanism for hydrogen in olivine. *Physics and Chemistry of Minerals*, 19, 460–471.
- Bali, E., Bolfan-Casanova, N., and Koga, K.T. (2008) Pressure and temperature dependence of H solubility in forsterite: An implication to water activity in the Earth interior. *Earth and Planetary Science Letters*, 268, 354–363.
- Bartelmebs, K.L., Boisen Jr., M.B., Gibbs, G.V., and Downs, R.T. (1993) Interactive computer software used in teaching and research in mineralogy at Virginia Tech. Geological Society of America Fall Meeting, Boston, A-347.
- Bell, D., Rossman, G.R., Maldener, J., Endisch, J., and Rauch, F. (2003) Hydroxide in olivine: a quantitative determination of the absolute amount and calibration of the IR spectrum. *Journal of Geophysical Research: Solid Earth*, 108, 2105, DOI: 10.1029/2001JB000679.
- Braithwaite, J.S., Wright, K., and Catlow, C.R.A. (2003) A theoretical study of the energetics and IR frequencies of hydroxyl defects in forsterite. *Journal of Geophysical Research: Solid Earth*, 112, 2284, DOI: 10.1029/2002JB002126.
- Chopelas, A. (1990) Thermal properties of forsterite at mantle pressures derived from vibrational spectroscopy. *Physics and Chemistry of Minerals*, 17, 149–156.
- (1991) Single crystal Raman spectra of forsterite, fayalite, and monticellite. *American Mineralogist*, 76, 1101–1109.
- Cromer, D.T. and Mann, J. (1968) X-ray scattering factors computed from numerical Hartree-Fock wave functions. *Acta Crystallographica*, A24, 321–325.
- Durben, D.J., McMillan, P.F., and Wolf, G.H. (1993) Raman study of the high-pressure behavior of forsterite (Mg_2SiO_4) crystal and glass. *American Mineralogist*, 78, 1143–1148.
- Gillet, P., Richet, P., Guyot, F., and Fiquet, G. (1991) High-temperature thermodynamic properties of forsterite. *Journal of Geophysical Research*, 96, 11805–11816.
- Iishi, K. (1978) Lattice dynamics of forsterite. *American Mineralogist*, 63, 1198–1208.
- Inoue, T., Weidner, D.J., Northrup, P.A., and Parise, J.B. (1998) Elastic properties of hydrous ringwoodite (γ -phase) in Mg_2SiO_4 . *Earth and Planetary Science Letters*, 160, 107–113.
- Jacobsen, S.D. and Smyth, J.R. (2006) Effect of water on the sound velocities of ringwoodite in the transition zone. In S. van der Lee and S.D. Jacobsen, Eds., *Earth's Deep Water Cycle*, 168, p. 131–145. American Geophysical Union Monograph Series, Washington, D.C.
- Jacobsen, S.D., Demouchy, S., Frost, D.J., Boffa-Ballaran, T., and Kung, J. (2005) A systematic study of OH in hydrous wadsleyite from polarized FTIR spectroscopy and single-crystal X-ray diffraction: Oxygen sites for hydrogen storage in the Earth's interior. *American Mineralogist*, 90, 61–70.
- Khisina, N.R., Wirth, R., Andrut, M., and Ukhanov, A.V. (2001) Extrinsic and intrinsic mode of hydrogen occurrence in natural olivines: FTIR and TEM investigation. *Physics and Chemistry of Minerals*, 28, 291–301.
- Kleppe, A.K. and Jephcoat, A.P. (2006) Raman spectroscopic studies of hydrous and nominally anhydrous deep mantle phase. In S. van der Lee and S.D. Jacobsen, Eds., *Earth's Deep Water Cycle*, 168, 69–93. Geophysical Union Monograph Series, Washington, D.C.
- Kleppe, A.K., Jephcoat, A.P., and Ross, N.L. (2001) Raman spectroscopic studies of phase E to 19 GPa. *American Mineralogist*, 86, 1275–1281.
- Kleppe, A.K., Jephcoat, A.P., and Smyth, J.R. (2002) Raman spectroscopic study of hydrous γ - Mg_2SiO_4 to 56.5 GPa. *Physics and Chemistry of Minerals*, 29, 473–476.
- (2006) High-pressure Raman spectroscopic study of Fo_{90} hydrous wadsleyite. *Physics and Chemistry of Minerals*, 32, 700–709.
- Koch-Müller, M., Dera, P., Fei, Y., Reno, B., Sobolev, N., Hauri, H.E., and Wysoczanski, R. (2003) OH⁻ in synthetic and natural coesite. *American Mineralogist*, 88, 1436–1445.
- Koch-Müller, M., Matsyuk, S.S., Rhede, D., Wirth, R., and Khisina, N. (2006) Hydroxyl in mantle olivine xenocrysts from the Udachnaya kimberlite pipe. *Physics and Chemistry of Minerals*, 33, 276–287.
- Kohlstedt, D.L., Keppler, H., and Rubie, D.C. (1996) The solubility of water in α , β , and γ phases of $(\text{Mg,Fe})_2\text{SiO}_4$. *Contributions to Mineralogy and Petrology*, 123, 345–357.
- Lam, P.K., Yu, R., Lee, M.W., and Sharma, S.K. (1990) Structural distortion and vibrational modes in Mg_2SiO_4 . *American Mineralogist*, 75, 109–119.
- Lemaire, C., Kohn, C.S., and Brooker, A.R. (2004) The effect of silica activity on the incorporation mechanisms of water in synthetic forsterite: A polarized infrared spectroscopic study. *Contributions to Mineralogy and Petrology*, 147, 48–57.
- Libowitzky, E. (1999) Correlation of O-H stretching frequencies and O-H...O bond lengths in minerals. *Monatshefte für Chemie*, 130, 1047–1059.
- Lin, C.C., Liu, L.G., and Irifune, T. (1999) High-pressure Raman spectroscopic study of chondrodite. *American Mineralogist*, 26, 226–233.
- Lin, C.C., Liu, L.G., Mernagh, T.P., and Irifune, T. (2000) Raman spectroscopic study of hydroxyl-clinohumite at various pressures and temperatures. *Physics and Chemistry of Minerals*, 27, 320–331.
- Litasov, K.D., Ohtani, E., Kagi, H., Jacobsen, S.D., and Ghosh, S. (2007) Temperature dependence and mechanism of hydrogen incorporation in olivine at 12.5–14.0 GPa. *Geophysical Research Letters*, 34, L16314.
- Mackwell, S.J. and Kohlstedt, D.L. (1990) Diffusion of hydrogen in olivine: implications for water in the mantle. *Journal of Geophysical Research*, 95, 5079–5088.
- Matsyuk, S.S. and Langer, K. (2004) Hydroxyl in olivines from mantle xenoliths in kimberlites of the Siberian platform. *Contributions to Mineralogy and Petrology*, 147, 413–437.
- Matveev, H., O'Neill, H.St.C., Ballhaus, C., Taylor, W.R., and Green, D.H. (2001) Effect of silica activity on OH-IR spectra of olivine: Implications for low- $a\text{SiO}_2$ mantle metasomatism. *Journal of Petrology*, 42, 721–729.
- Mei, S. and Kohlstedt, D.L. (2000a) Influence of water on plastic deformation of olivine aggregates, 1. Diffusion creep regime. *Journal of Geophysical Research*, 105, 21457–21469.
- (2000b) Influence of water on plastic deformation of olivine aggregates, 2. Dislocation creep regime. *Journal of Geophysical Research*, 105, 21471–21481.
- Miller, G.H., Rossman, G.R., and Harlow, G.E. (1987) The natural occurrence of hydroxide in olivine. *Physics and Chemistry of Minerals*, 14, 461–472.
- Mosenfelder, J.L., Deligne, N.I., Asimow, P.D., and Rossman, G.R. (2006) Hydrogen incorporation in olivine from 2–12 GPa. *American Mineralogist*, 9, 285–294.
- Paques-Ledent, M.T. and Tarte, P. (1973) Vibrational studies of olivine-type compounds. I. The IR and Raman spectra of the isotopic species of Mg_2SiO_4 . *Spectrochimica Acta*, 29A, 1007–1016.
- Pirou, B. and McMillan, P. (1983) The high-frequency vibrational spectra of vitreous and crystalline orthosilicates. *American Mineralogist*, 68, 426–443.
- Rossman, G.R. and Smyth, J.R. (1990) Hydroxyl contents of accessory minerals in mantle eclogites and related rocks. *American Mineralogist*, 75, 775–780.
- Sheldrick, M.G. (1997) SHELX-97, Program for crystal structure refinement. Göttingen University, Germany.
- Skogby, H., Bell, D.R., and Rossman, G.R. (1990) Hydroxide in pyroxene: variations in the natural environment. *American Mineralogist*, 75, 764–774.
- Smyth, J.R. (1987) β - Mg_2SiO_4 : A potential host for water in the mantle? *American Mineralogist*, 72, 1051–1055.
- (1988) Electrostatic characterization of oxygen sites in minerals. *Geochimica et Cosmochimica Acta*, 53, 1101–1110.
- (1994) A crystallographic model for hydrous wadsleyite: An ocean the Earth's interior? *American Mineralogist*, 79, 1021–1025.
- (2006) Hydrogen in high pressure silicate and oxide mineral structures. In H. Keppler and J.R. Smyth, Eds., *Water in Nominally Anhydrous Minerals*, 62, p. 85–116. Reviews in Mineralogy and Geochemistry, Mineralogical Society of America, Chantilly, Virginia.
- Smyth, J.R. and Jacobsen, S.D. (2006) Nominally anhydrous minerals and Earth's deep water cycle. In S. van der Lee and S.D. Jacobsen, Eds., *Earth's Deep Water Cycle*, 168, p. 1–11. American Geophysical Union Monograph Series, Washington, D.C.
- Smyth, J.R., Kawamoto, T., Jacobsen, S.D., Swope, J.R., Hervig, R.L., and Holloway, J.R. (1997) Crystal structure of monoclinic hydrous wadsleyite [β - $(\text{Mg,Fe})_2\text{SiO}_4$]. *American Mineralogist*, 82, 270–275.
- Smyth, J.R., Frost, D.J., and Nestola, F. (2005) Hydration of olivine and the Earth's

- deep water cycle. *Geochimica et Cosmochimica Acta Supplement*, 69, Supplement 1, Goldschmidt Conference Abstracts 2005, p. A746.
- Smyth, J.R., Frost, D.J., Nestola, F., Holl, C.M., and Bromiley, G. (2006) Olivine hydration in the deep upper mantle: Effects of temperature and silica activity. *Geophysical Research Letters*, 33, L15301.
- Smyth, J.R., Mierdel, K., Keppler, H., Langenhorst, F., Dubrovinsky, L., and Nestola, F. (2007) Crystal chemistry of hydration in aluminous orthopyroxene. *American Mineralogist*, 92, 973–976.
- Tokonami, M. (1965) Atomic scattering factor for O^{2-} . *Acta Crystallographica*, 19, 486.
- Van de Moortèle, B., Reynard, B., McMillan, P.F., Wilson, M., Beck, P., Gillet, P., and Jahn, S. (2007) Shock-induced transformation of olivine to a new metastable $(Mg,Fe)_2SiO_4$ polymorph in Martian meteorites. *Earth and Planetary Science Letters*, 261, 469–475.
- Walker, A.M., Hermann, J., Berry, A.J., and O'Neill, H.St.C. (2007) Three water sites in upper mantle olivine and the role of titanium in the water weakening mechanism. *Journal of Geophysical Research*, 112, B05211.
- Wang, S.Y., Sharma, S.K., and Cooney, T.F. (1993) Micro-Raman and infrared spectral study of forsterite under high pressure. *American Mineralogist*, 78, 469–476.
- Withers, C.A., Wood, B.J., and Carroll, M.R. (1998) The OH content of pyrope at high pressure. *Chemical Geology*, 47, 161–171.
- Zhao, Y.-H., Ginsberg, B.S., and Kohlstedt, L.D. (2004) Solubility of hydrogen in olivine: dependence on temperature and iron content. *Contributions to Mineralogy and Petrology*, 147, 155–161.

MANUSCRIPT RECEIVED MARCH 27, 2008

MANUSCRIPT ACCEPTED JANUARY 27, 2009

MANUSCRIPT HANDLED BY PRZEMYSŁAW DERA